Soft Computing (2020) 24:16213–16223
https://doi.org/10.1007/s00500-020-04935-3

METHODOLOGIES AND APPLICATION

Physical significance of chemical processes and Lorentz's forces aspects on Sisko fluid flow in curved configuration

M. Ali[1] · M. Irfan[2] · W. A. Khan[3,4] · F. Sultan[1] · M. Shahzad[1] · M. Khan[2]

Published online: 18 April 2020

Abstract

Current determination is committed to characterize the features of curved surface for Sisko fluid in the presence of Lorentz's forces. Heat–mass relocation exploration is conducted in the presence of homogeneous–heterogeneous processes and non-uniform heat sink/source. Similarity variables are designated to transmute nonlinear PDEs into ODEs. These intricate ordinary differential expressions assessing the flow situation are handled efficaciously by manipulating bvp4c scheme. Graphical demonstration is deliberated to scrutinize the variation in pressure, velocity, temperature and concentration profiles with respect to flow regulating parameters. Numerical data are displayed through tables in order to surmise variation in surface drag force and heat transport rate. It is noted that radius of curvature and temperature-dependent heat sink/source significantly affect heat–mass transport mechanisms for curved surface. Furthermore, graphical analysis reveals that velocity profile of Sisko magneto-fluid enhances for augmented values of curvature parameter. Additionally, it is evaluated that increasing values of heat source parameter and Lorentz's forces, pressure profile exhibited the diminishing behavior.

Keywords Unsteady flow · Sisko fluid · Homogeneous–heterogeneous reactions · Non-uniform heat sink/source

List of symbols

r, s	Curvilinear coordinates
a, b, n	Material constants
E, F	Autocatalysts
G_a, G_b	Concentration of chemical species E and F
k_1, k_s	Rate coefficient of homogeneous and heterogeneous reactions
G_{a0}	Uniform concentration
B_0	Applied magnetic field
R	Radius of curvature
V	Velocity vector
u, v	Velocity components
ρ_f	Fluid density
K	Thermal conductivity
T	Temperature of fluid
T_w	Temperature at the wall
T_∞	Ambient temperature
q_r	Radiative heat flux
D_A, D_B	Diffusion coefficients of two species (E, F)
q'''	Heat sink/source
C	Constant
α_1	Thermal diffusivity
U_w	Stretching velocity
P	Pressure
A^*	Space dependent
B^*	Temperature dependent
η	Dimensionless variable
ψ	Stream function
P	Dimensionless pressure
R_d	Radiation parameter
F	Dimensionless velocity
θ	Dimensionless temperature
φ	Dimensionless concentration
δ	Unsteadiness parameter
M	Magnetic parameter

Communicated by V. Loia.

✉ W. A. Khan
waqar_qau85@yahoo.com; waqarazeem@bit.edu.cn

[1] Department of Mathematics and Statistics, Hazara University, Mansehra 21300, Pakistan

[2] Department of Mathematics, Quaid-I-Azam University, Islamabad 44000, Pakistan

[3] School of Mathematics and Statistics, Beijing Institute of Technology, Beijing 100081, China

[4] Department of Mathematics, Mohi-ud-Din Islamic University, Nerian Sharif, Azad Kashmir 12010, Pakistan

ε	Diffusion coefficient
Pr	Generalized Prandtl number
k_2	Strength coefficient homogenous reaction
Sc	Generalized Schmidt number
K	Dimensionless radius of curvature
A	Material parameter of the Sisko fluid
γ	Generalized Biot number
τ_w	Surface shear stress
q_w	Surface heat flux
C_f	Skin friction coefficient
Nu_s	Local Nusselt number
$\mathrm{Re}_a, \mathrm{Re}_b$	Local Reynolds numbers

1 Introduction

Currently, the term catalysis isolates the connections loosening progression through which chemical fusions are occurred mutually. Catalysis advances materializes via heterogeneous–homogeneous expansions. The mass transport phenomenon considering the aspects of chemical processes (heterogeneous/homogeneous) has an essential use in biological structure. Numerous multifaceted relations can arise between homogeneous–heterogeneous processes. These processes progress gradually or not all collectively deprived of any catalyst. However, these reactions have competence to respond much hurriedly with catalyst. Furthermore, a quantity of collective uses of chemical processes comprises porcelains, fog materialization and diffusion, unindustrialized and industrialized regions, etc. Few studies based on influence of these processes were conferred via Refs. (Chaudhary and Merkin 1995; Merkin 1996; Khan et al. 2018; Xu et al. 2018; Irfan et al. 2018; Hayat et al. 2018). The chemical processes properties in micropolar fluid in cone reported by Mahdy (2019). In curved surface, the influence of chemical species with radiative second-grade fluid was examined by Imtiaz et al. (2019). Recently, numerically study on ferromagnetic chemically reactive flow was scrutinized by Waqas (2020). He established that the homogeneous–heterogeneous parameters fall off the concentration of micropolar fluid. He noted that the ferro-hydro-dynamic interaction parameter has conflicted performance on thermal and velocity field.

Recent advances clarify that owing to widespread and developing uses the non-Newtonian fluids have attained noteworthy thought in engineering (Zhao et al. 2016; Deng et al. 2017a, b, c; Zhao et al. 2017; Deng et al. 2019; Zhao et al. 2019a, b; Zhao et al. 2020; Hei et al. 2019; Zhang et al. 2019) bio-chemical and genetic properties for instance pharmacological substances, polymer waters, synovial liquefied, etc. The auspicious sorts of non-Newtonian liquids (Khan et al. 2017; Mahanthesh et al. 2018; Soomro et al. 2018; Anwar and Rasheed 2018; Rashid et al. 2019; Asghar et al. 2019; Waqas et al. 2019; Khan et al. 2019) and unpredictability of flow in natural surroundings, innumerable nonlinear associations have been proposed by scientists to explore the physical aspects of these non-Newtonian liquids. The Sisko fluid model is the sort of generalized Newtonian fluids which associate the species of power law and viscous models, respectively. Khan et al. (2016) reported numerically the performance of non-Fourierís and Fickís laws on Sisko liquid model. Shen et al. (2018) studied transient Sisko nanomaterial with Cattaneo heat transport. Their assessment established that to explore the augmentation of abnormal thermal conductivity Caputo time fractional derivatives are additional proficient. The chemical species aspects on Sisko fluid was analyzed by Malik and Khan (2018). They scrutinized that concentration of Sisko fluid fall off for heterogeneous parameter. Currently, in diverse veins the blood flow considering nonlinear Sisko fluid was examined by Toghraie et al. (2020). Their theory identified that in the dominant vein area the heat fluxes impact is deserted.

Here, we scrutinize the properties of chemical species on radiated Sisko curved surface via bvp4c approach (Khan et al. 2019a, b; Sultan et al. 2019; Muhammad et al. 2019; Haq et al. 2019; Ali et al. 2019a, b, 2020; Sultan et al. 2019; Shahzad et al. 2020). The convective phenomenon, magnetic and non-uniform heat sink/source aspects are incorporated. Outcomes of influential parameters are conferred via graphs.

2 Problem formulation

Here, an electrically conducting Sisko material in curved configuration is considered. Geometry of presented physical model in curvilinear coordinate is presented through Fig. 1. Features of viscous dissipation are retained. Characteristics of homogeneous–heterogeneous processes are accounted. The geometry of the presented problem depends on R. Moreover, heated liquid behind sheet is operated to heat up the stretched surface by convective mode of heat transport.

The quartic autocatalysis for isothermal reaction is given by

$$E + 2F \rightarrow 3F, \quad \text{rate} = k_1 G_a G_b^2, \tag{1}$$

While on catalytic surface the isothermal reaction is single reaction and first order is

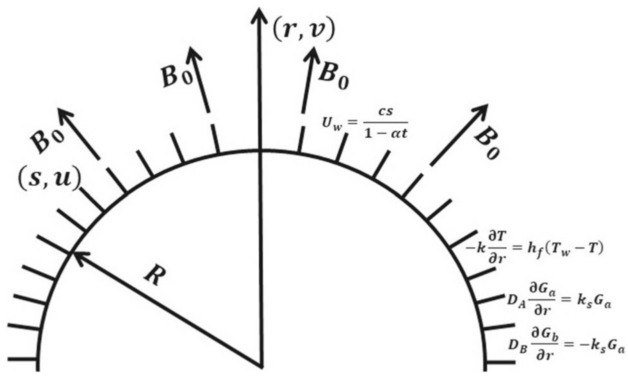

Fig. 1 Flow geometry

$$E \to F, \quad \text{rate} = k_s G_a, \tag{2}$$

Note that the relationship of Eq. (1) specifies reaction rate at far field is zero, so does it at the external edge of related layer. By employing overhead assumptions, the governing the physical problem is written as:

$$\frac{\partial}{\partial r}(rv) + \frac{\partial}{\partial r}(Rv) + R\frac{\partial u}{\partial s} = 0, \tag{3}$$

$$\frac{\partial p}{\partial r} = \rho_f\left(\frac{u^2}{r+R}\right), \tag{4}$$

$$\begin{aligned}&\frac{\partial u}{\partial t} + v\frac{\partial u}{\partial r} + u\left(\frac{R}{r+R}\right)\frac{\partial u}{\partial s} + uv\left(\frac{1}{r+R}\right)\\ &= -\frac{1}{\rho_f}\left(\frac{R}{r+R}\right)\frac{\partial p}{\partial s} + \frac{a}{\rho_f(r+R)^2}\\ &\times\frac{\partial}{\partial r}\left[(r+R)^2\frac{\partial u}{\partial r} - u(r+R)^2\left(\frac{1}{r+R}\right)\right]\\ &+\frac{b}{\rho_f(r+R)^2}\frac{\partial}{\partial r}\left[(r+R)^2\times\left(\frac{\partial u}{\partial r} - \frac{u}{r+R}\right)^n\right] - \frac{\sigma B_0^2}{\rho_f}u,\end{aligned} \tag{5}$$

$$\begin{aligned}\frac{\partial T}{\partial t} + v\frac{\partial T}{\partial r} + u\left(\frac{R}{r+R}\right)\frac{\partial T}{\partial s} = \alpha_1\frac{\partial^2 T}{\partial r^2} + \alpha_1\left(\frac{1}{r+R}\right)\frac{\partial T}{\partial r}\\ - \frac{1}{(r+R)}\frac{\partial}{\partial r}(r+R)\,q_r\\ + q''',\end{aligned} \tag{6}$$

$$\frac{\partial G_a}{\partial t} + v\frac{\partial G_a}{\partial r} + \frac{Ru}{r+R}\frac{\partial G_a}{\partial s} = D_A\left(\frac{\partial^2 G_a}{\partial r^2} + \frac{1}{r+R}\frac{\partial G_a}{\partial r}\right) - k_1 G_a G_b^2, \tag{7}$$

$$\begin{aligned}&\frac{\partial G_b}{\partial t} + v\frac{\partial G_b}{\partial r} + u\left(\frac{R}{r+R}\right)\frac{\partial G_b}{\partial s}\\ &= D_B\left(\frac{\partial^2 G_b}{\partial r^2} + \frac{1}{r+R}\frac{\partial G_b}{\partial r}\right) + k_1 G_a G_b^2,\end{aligned} \tag{8}$$

with

$$\begin{aligned}&u = U_w(s) = \frac{as}{1-\alpha t},\ v = 0, \quad k_f\frac{\partial T}{\partial r} = h(T_f - T),\\ &D_A\frac{\partial G_b}{\partial r} = -D_B\frac{\partial G_b}{\partial r} = k_s G_a \text{ at } r = 0,\end{aligned} \tag{9}$$

$$u \to 0,\ \frac{\partial u}{\partial r} \to 0,\ T \to T_\infty,\ G_a \to G_0,\ G_b \to 0 \quad \text{as } r \to \infty. \tag{10}$$

Non-uniform heat sink/source and radiative heat flux are estimated as

$$q''' = \frac{kU_s(s,t)}{sv}\left[A^*(T_w - T_\infty)f' + (T - T_\infty)B^*\right], \tag{11}$$

$$q_r = -\frac{16\sigma^* T_\infty^3}{3k^*}\frac{\partial T}{\partial r}, \tag{12}$$

invoking Eqs. (11) and (12) into Eq. (6), we get

$$\begin{aligned}&\frac{\partial T}{\partial t} + v\frac{\partial T}{\partial r} + u\left(\frac{R}{r+R}\right)\frac{\partial T}{\partial s}\\ &+\frac{kU_s(s,t)}{sv}\left[A^*(T_w - T_\infty)f' + (T - T_\infty)B^*\right].\end{aligned} \tag{13}$$

Considering

$$\begin{aligned}&u = U_w f'(\eta),\ v = -U_w\left(\frac{R}{r+R}\right)Re_b^{-\frac{1}{n+1}}\left[\frac{2n}{n+1} + \left(\frac{1-n}{1+n}\right)\eta f'(\eta)\right],\\ &\Psi = sU_w Re_b^{-\frac{1}{n+1}} f(\eta),\ \theta(\eta) = \frac{T - T_\infty}{T_f - T_\infty},\ G_a = G_\infty\varphi(\eta),\ G_b = G_\infty\vartheta(\eta),\\ &p = \frac{\rho a^2 s^2}{(1-\alpha t)^2}P(\eta),\ \eta = \frac{r}{s}Re_b^{\frac{1}{n+1}}.\end{aligned} \tag{14}$$

Utilizing the overhead transformations, the requirement of Eq. (1) is automatically fulfilled and Eqs. (4) and (5) take the form

$$\frac{\partial P}{\partial \eta} = \frac{f'^2}{\eta + K}, \tag{15}$$

$$\begin{aligned}&\frac{2K}{\eta+K}P = \frac{K}{\eta+K}\left(\frac{2n}{n+1}\right)\left(ff'' + \frac{1}{\eta+K}ff'\right) - \frac{K}{\eta+K}f'^2\\ &+A\left[f''' - \frac{1}{(\eta+K)^2}f' + \frac{1}{\eta+K}f''\right]\\ &+n\left(f'' - \frac{1}{\eta+K}f'\right)^{n-1}\left(f''' + \frac{1}{(\eta+K)^2}f' - \frac{1}{\eta+K}f''\right)\\ &+\frac{2}{\eta+K}\left(f'' - \frac{1}{\eta+K}f'\right)^n - Mf' - \delta\left[f' + \left(\frac{2-n}{n+1}\right)\eta f''\right],\end{aligned} \tag{16}$$

Eliminating contribution of pressure from Eqs. (15) and (16), then governing boundary layer expression of Sisko fluid with heat and mass transfer is expressed as follows

$$A\left[f'''' + \frac{2}{\eta+K}f''' - \frac{1}{(\eta+K)^2}f' + \frac{1}{(\eta+K)^3}f'\right]$$
$$+\left(\frac{2n}{n+1}\right)\left[\frac{K}{\eta+K}(ff'' + f'f'')\right.$$
$$\left. + \frac{K}{(\eta+K)^2}(ff'' + f'^2) - \frac{K}{(\eta+K)^2}ff'\right] - \frac{2K}{\eta+K}f'f''$$
$$-\frac{2K}{(\eta+K)^2}f'^2 + n\left(f'' - \frac{1}{\eta+K}f'\right)^{n-1}$$
$$\times\left(f'''' + \frac{1}{(\eta+K)^2}f'' - \frac{1}{(\eta+K)^3}f'\right)$$
$$+n(n-1)\left(f'' - \frac{1}{\eta+K}f'\right)^{n-2}$$
$$\left(f''' - \frac{1}{\eta+K}f'' + \frac{1}{(\eta+K)^2}f'\right)^2$$
$$+2n\left(f'' - \frac{1}{\eta+K}f'\right)^{n-1}$$
$$\left(\frac{1}{\eta+K}f''' - \frac{1}{(\eta+K)^2}f'' + \frac{1}{(\eta+K)^3}f'\right)$$
$$-M\left(f'' + \frac{1}{\eta+K}f'\right) - \frac{\delta}{\eta+K}\left[f' + \frac{2-n}{n+1}\eta f''\right]$$
$$-\delta\left[\frac{2-n}{n+1}\eta f''' + \frac{3}{n+1}f''\right] = 0, \tag{17}$$

$$\theta'' + \frac{1}{\eta+K}\theta' + \Pr Nr \times \left(\frac{K}{\eta+K}\right)\left(\frac{2n}{n+1}\right)f\theta' - \Pr Nr\delta\left(\frac{n-2}{n+1}\right)\eta\theta' = 0, \tag{18}$$

$$\varphi'' + \left(\frac{1}{\eta+K}\right)\varphi' + \mathrm{Sc}\left[\frac{K}{\eta+K}f\varphi' - \delta\left(\frac{n-2}{n+1}\right)\eta\varphi' + k_2\varphi\vartheta^2\right] = 0, \tag{19}$$

$$\vartheta'' + \left(\frac{1}{\eta+K}\right)\vartheta' + \frac{\mathrm{Sc}}{\varepsilon}\left[\frac{K}{\eta+K}f\vartheta' - \delta\left(\frac{n-2}{n+1}\right)\eta\vartheta'' - k_2\varphi\vartheta^2\right] = 0, \tag{20}$$

$$f(0) = 0, f'(0) = 1, \theta''(0) = \gamma(1-\theta'(0)), \varphi'(0) = -\varepsilon\varphi'(0) = k_s\vartheta(0), \tag{21}$$

$$f'(\infty) = 0, f''(\infty) = 0, \theta(\infty) = 0, \varphi(\infty) = 1, \tag{22}$$

physical parameters involved in the problem are represented as follows

$$Re_a = \frac{U_w s\rho_f}{a},\ Re_b = \frac{U_w^{2-n}s^n\rho_f}{b},\ A = \frac{Re_b^{\frac{2}{n+1}}}{Re_a},\ M = \frac{\sigma B_0^2}{(\rho c)_f}(1-\alpha t),$$
$$K = \frac{R}{s(1-\alpha t)}Re_b^{\frac{1}{n+1}},\ \delta = \frac{\alpha}{a},\ \mathrm{Nr} = \frac{3R_d}{4+3R_d},\ R_d = \frac{kk^*}{4\sigma^* T_\infty^3},$$
$$\alpha_1 = \frac{k}{(\rho c_p)_f},\ \Pr = \frac{sU_w}{\alpha_1}Re_b^{-\frac{2}{n+1}},\ Sc = \frac{sU_w}{D_B}Re_b^{-\frac{2}{n+1}},\ k_2 = \frac{k_1 G_\infty(1-\alpha t)}{a}. \tag{23}$$

For simplicity, we assume

$$\vartheta(\eta) + \varphi(\eta) = 1. \tag{24}$$

By utilizing Eq. (18), one obtains

$$\varphi'' + \left(\frac{1}{\eta+K}\right)\varphi' + \mathrm{Sc}\left[\frac{K}{\eta+K}f\varphi' - \delta\left(\frac{n-2}{n+1}\right)\eta\varphi' + k_2\varphi(1-\varphi)^2\right] = 0, \tag{25}$$

2.1 Drag force and rate of heat–mass transport

Mathematically

$$C_f = \frac{\tau_w}{\frac{1}{2}\rho_f U_w^2},\ \text{with}\ \tau_w = \mu\left(\frac{\partial u}{\partial r} - \frac{u}{(r+R)}\right)\bigg|_{r=0}, \tag{26}$$

$$\mathrm{Nu}_s = \frac{q_m s}{k(T_f - T_\infty)},\ \text{with}\ q_m = -k\left(1 + \frac{16\sigma^* T_\infty^3}{3kk^*}\right)\frac{\partial T}{\partial r}\bigg|_{r=0}. \tag{27}$$

Utilizing the non-dimensional variables, we obtain

$$\frac{1}{2}Re_b^{\frac{1}{n+1}}C_f = A\left[f''(0) - \frac{f''(0)}{K}\right] + \left[f''(0) - \frac{f'(0)}{K}\right]^n, \tag{28}$$

$$Re_b^{-\frac{1}{n+1}}\mathrm{Nu}_s = -\frac{\theta'(0)}{Nr}. \tag{29}$$

3 Numerical solutions

Set of Eqs. (17)–(22) along with associated conditions are tackled numerically via MATLAB tool bvp4c. For this scheme boundary value problem is rehabilitated into initial value problem and MATLAB software bvp4c is implemented for step by step integrated.

4 Discussion

Main theme of this research work is to mark the physical interpretation of behavior of various physical parameters which arise in flow, heat and mass transport of Sisko magneto-fluid past a curved stretched surface. Numerical technique namely bvp4v is employed to integrate. Main

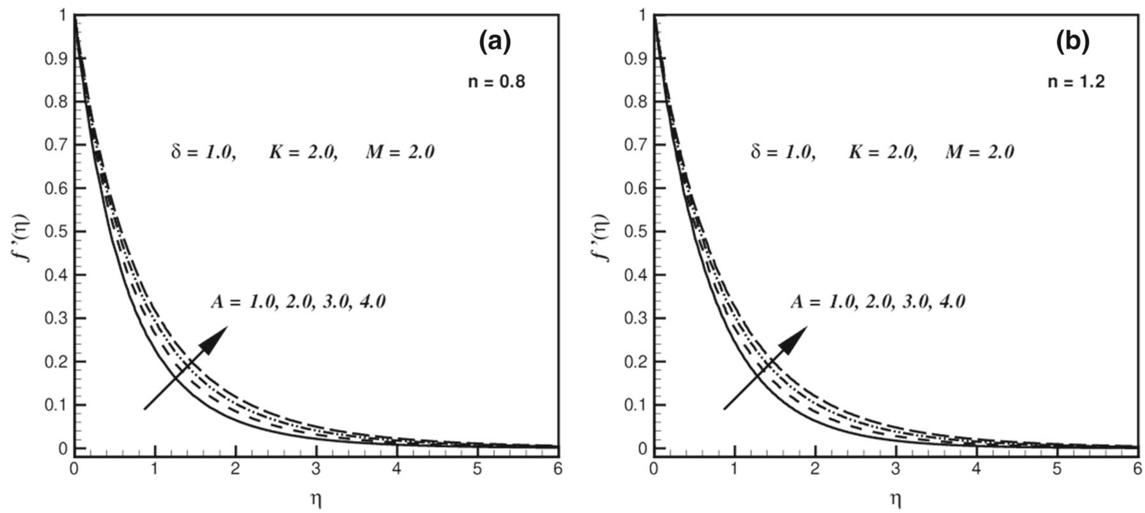

Fig. 2 a, b $f'(\eta)$ via A for $n<1$ and $n>1$

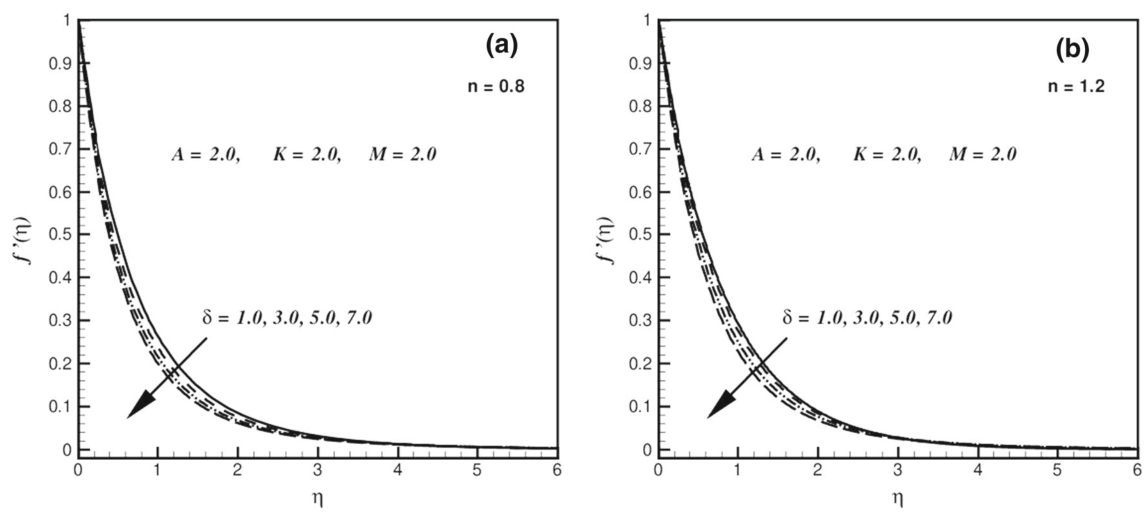

Fig. 3 a, b $f'(\eta)$ via δ for $n<1$ and $n>1$

motivation behind current research work is to investigate the aspect of all arising physical parameters on velocity, temperature and concentration profiles. Moreover, flow and heat transport mechanisms are probed by computing the value of drag forces and Nusselt number.

4.1 Velocity profiles

Features of A, δ, K and M via Figs. 2, 3, 4 and 5 are communicated in this subsection for $n<1$ and $n>1$. Figure 2a and b represents the significant effect A on velocity of Sisko fluid for curved stretched surface. Through graphical data, outcomes are substantial in case of $n<1$. Physical enhancement conducts with A due to low shear rate and high shear rate for low viscosity regarding Sisko fluid flow. The non-dimensional velocity of Sisko fluid for δ is sketched through Fig. 3a and b with raising values of time-dependent parameter δ. As revealed from graphical data, δ has great impact on velocity of magneto-fluid, i.e., velocity of magneto-fluid deteriorates by raise in δ. Figure 4a and b visualizes that augmented values of K has a great impact on velocity for $n<1$ as well as for $n>1$. It is observed that Sisko fluid and its momentum boundary layer enhances for augmented values of K. Moreover, we can detect from our graphical data that results are more prominent for shear thinning fluid as compared to shear thickening fluid. Figures 5a and b demarcates the inspiration of M on velocity of Sisko fluid. One can explicitly observe that momentum boundary layer declines for incrementing values of M.

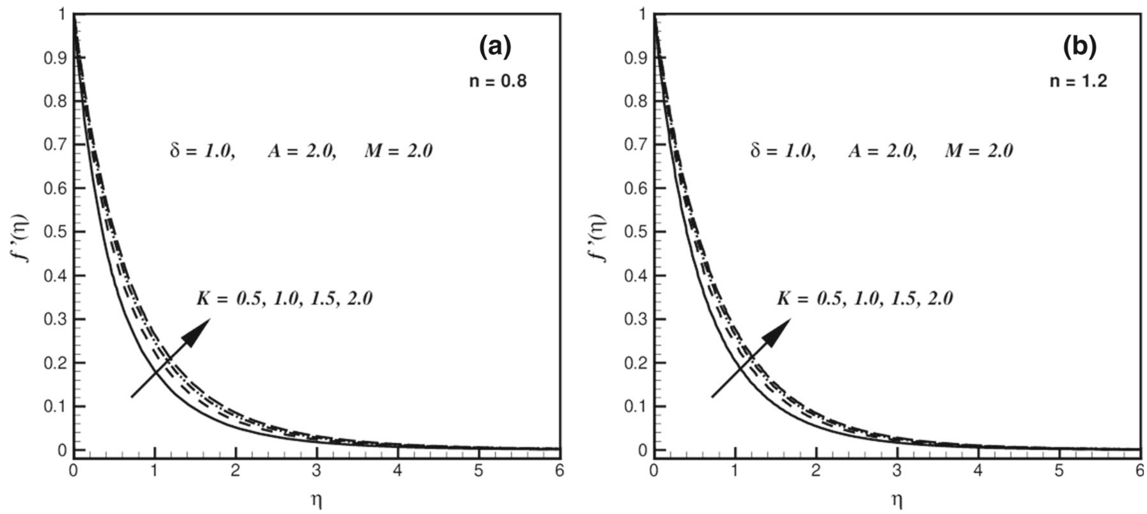

Fig. 4 a, b: $f'(\eta)$ via K for $n<1$ and $n>1$

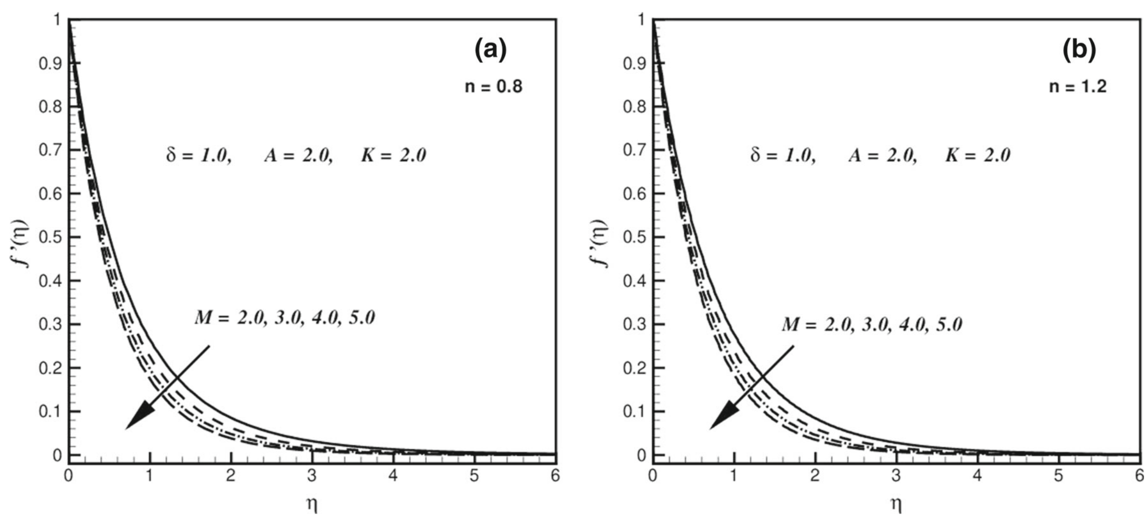

Fig. 5 a, b $f'(\eta)$ via M for $n<1$ and $n>1$

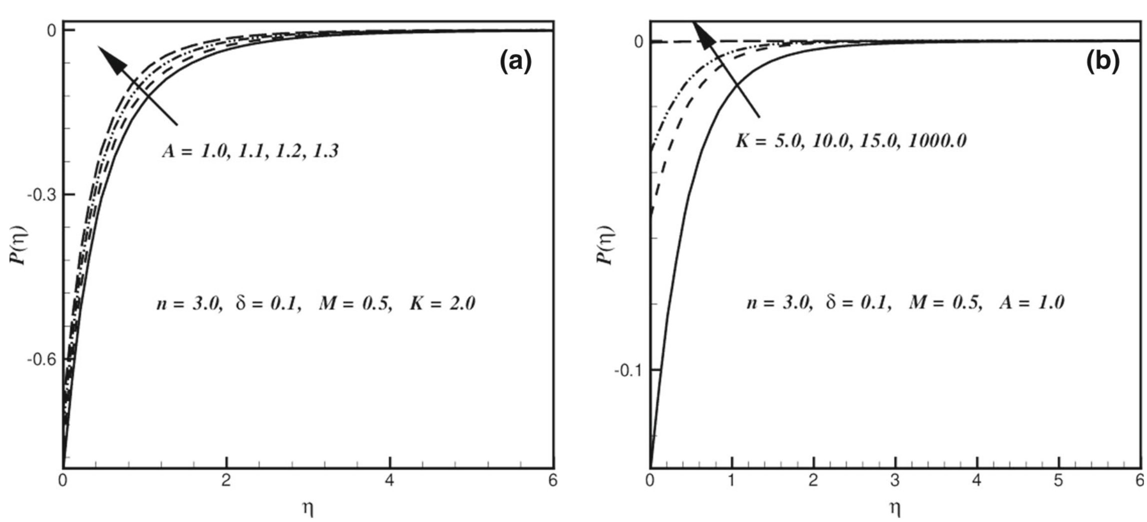

Fig. 6 a, b $P(\eta)$ via A for $n<1$ and K for $n>1$

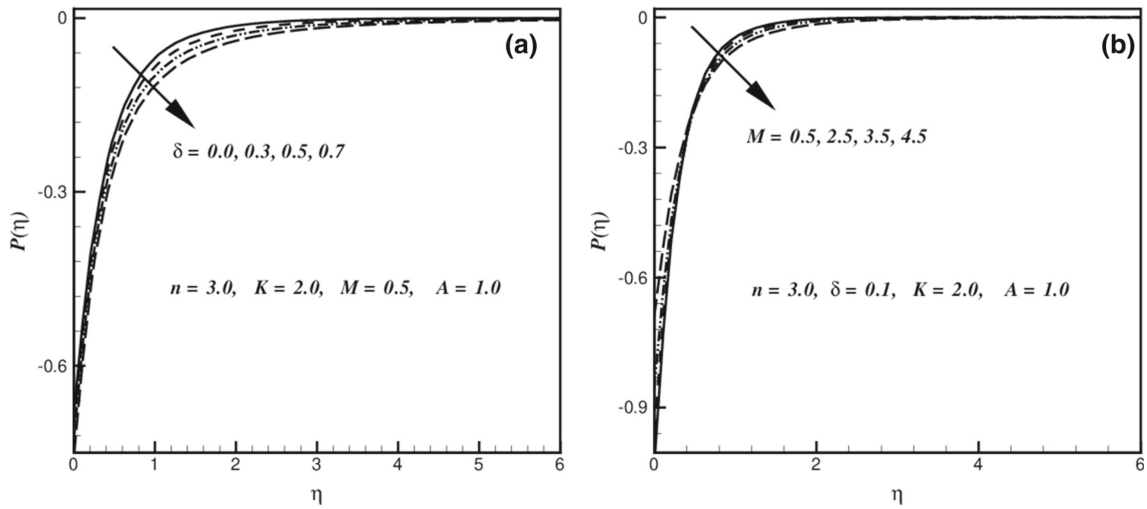

Fig. 7 a, b $P(\eta)$ via δ for $n<1$ and M for $n<1$

4.2 Pressure profile

Figures 6 and 7 illustrate the aspects of various physical parameter on pressure profile inside the boundary region for $n > 1$. Figure 6a is devoted to illuminate the bearing of A on Sisko fluid. One can detect from these pressure profiles that inside the boundary layer region pressure profile raises with boosts values of A. Moreover, pressure profile inside boundary layer enhances with raising values of K and is detected through Fig. 6b. We also observed from our data that curved surface become planner surface for augmented values of K and pressure inside boundary layer approaches to zero. Curved surface becomes more curved for smaller value of K. This behavior of K can explained on basis that curvature of surface raises due to curvilinear nature of flow. Furthermore, variation of pressure distribution for different values of unsteady parameters δ and magnetic parameter M is demonstrated through Fig. 7a and b. We can perceive from our data that pressure profile inside the boundary layer deteriorate with boosts values of δ and M.

4.3 Temperature profile

Figures 8 and 9 illustrate the aspects of various physical on the temperature of Sisko fluid for $n<1$ and $n > 1$. Figures 8a and b and 9a and b scrutinize the pivotal effect of nonlinear heat source/sink parameter A^*(space dependent) and B^*(temperature dependent) on temperature of fluid. It is engrossed that there is considerable raise in temperature of Sisko fluid for growing values of A^* and B^*.

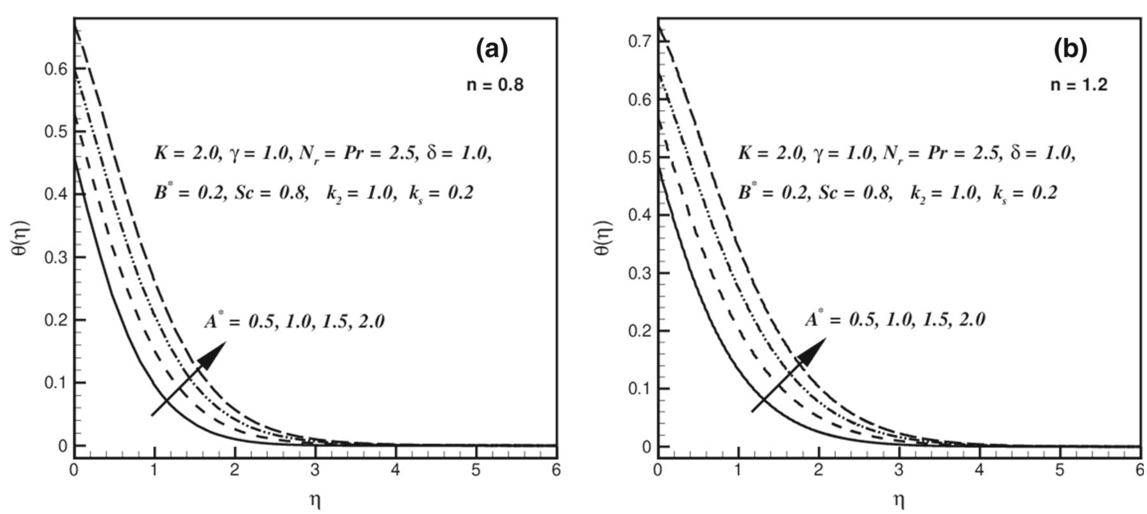

Fig. 8 a, b $\theta(\eta)$ via A^* for $n<1$ and $n > 1$

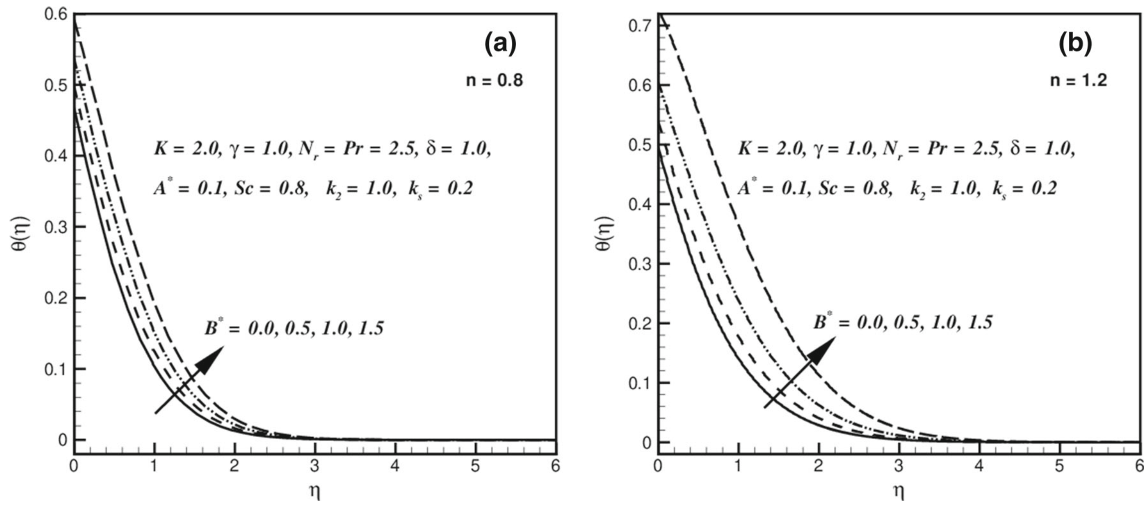

Fig. 9 a, b $\theta(\eta)$ via B^* for $n<1$ and $n>1$

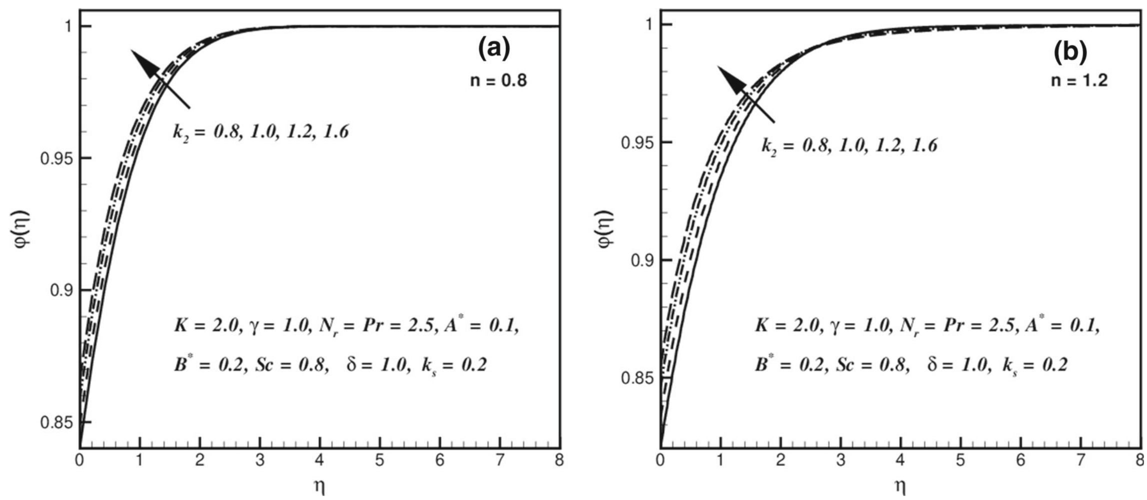

Fig. 10 a, b: $\phi(\eta)$ via k_2 for $n<1$ and $n>1$

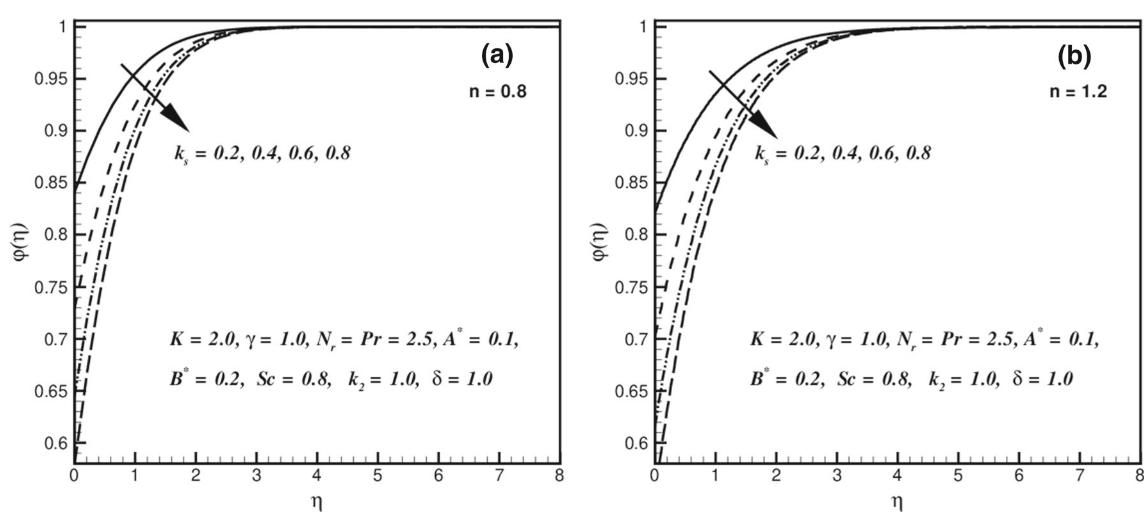

Fig. 11 a, b $\phi(\eta)$ via k_s for $n<1$ and $n>1$

Table 1 Numerical outcomes of $\frac{1}{2}Re_b^{-\frac{1}{n+1}}C_f$ for various physical parameters

δ	K	M	A	$\frac{1}{2}Re_b^{-\frac{1}{n+1}}C_f$
0.0	5.0	0.5	2.0	2.714143
0.3	–	–	–	2.764031
0.5	–	–	–	2.861142
0.6	5.5	–	–	2.940485
–	6.0	–	–	2.891498
–	6.5	–	–	2.850601
–	–	0.6	–	3.081705
–	–	0.8	–	3.233271
–	–	1.0	–	3.372492
–	–	–	2.2	3.147898
–	–	–	2.4	3.293177
–	–	–	2.6	3.436201

Table 2 Numerical outcomes of $Re_b^{-\frac{1}{n+1}}Nu_s$ for various physical parameters when $A = M = 2, Pr = 2.5, Sc = 3.0, k_s = 0.2, k_2 = 1$ and $N_r = 2.5$

δ	K	Nr	A^*	B^*	$Re_b^{-\frac{1}{n+1}}Nu_s$
0.0	2.0	1.8	0.1	0.2	0.0987053
0.1	–	–	–	–	0.143435
0.2	–	–	–	–	0.211845
0.4	3.0	–	–	–	0.312469
–	4.0	–	–	–	0.311058
–	5.0	–	–	–	0.310306
–	–	2.0	–	–	0.27587
–	–	2.5	–	–	0.205496
–	–	3.0	–	–	0.160364
–	–	–	0.3	–	0.130397
–	–	–	0.5	–	0.09929
–	–	–	0.7	–	0.0669757
–	–	–	–	0.4	0.128192
–	–	–	–	0.6	0.0933111
–	–	–	–	0.8	0.0534883

4.4 Concentration profile

Figures 10 and 11 display the features of k_2 and k_s on concentration of Sisko fluid. Impact of k_2 on concentration profile is presented through 10a and b. It is appraised from obtained data that concentration of Sisko fluid is rising function of k_2. Figure 11a and b reflects the behavior of concentration profile in response to variation in k_s. It elucidates that concentration profile deteriorates with the escalation in k_s.

4.5 Quantities of physical interest

Tables 1 and 2 are presented to demonstrate the impact of achieved outcomes for surface drag forces $\frac{1}{2}Re_b^{-\frac{1}{n+1}}C_f$ and heat transfer rate $Re_b^{-\frac{1}{n+1}}Nu_s$. It is noticed from Table 1 that magnitude of surface drag forces is greater for larger estimation of $\delta,\ M,\ A$ while opposite trend is observed for K. Table 2 reveals that magnitude of heat transport rate deteriorates for augmented values of $K,\ N_r,\ A^*$ and B^* while it rises for δ.

5 Main outcome

A detailed characterization of boundary layer flow and heat transport of Sisko fluid is studied here in order to elucidate the aspects of chemical process. Moreover, heat sink/source is utilized to describe the heat–mass transport mechanism. Numerical computation is employed for the modeled equations. Outcomes of current paper are presented in form of graphical and tabular data. The finding can be summarized as follows:

- Larger M and δ yield reduction in $f'(\eta)$.
- Pressure profile inside boundary region is increased when A and K are enhanced.
- Dimensionless curvature K and $\frac{1}{2}Re_b^{-\frac{1}{n+1}}C_f$ are inversely proportional.
- An increment in heat source/sink parameters A^* and B^* corresponds to rise up temperature and decreases heat transfer rate.
- The homogeneous reaction and isothermal cubic autocatalator kinetics, govern by first-order kinetics occurring ambient fluid.
- The model of chemical reaction is involved for mass transfer.

Acknowledgements This project was funded by the postdoctoral international exchange program for incoming postdoctoral students, at Beijing Institute of Technology, Beijing, China.

Compliance with ethical standards

Conflict of interest All authors declare that they have no conflict ofinterest.

References

Ali M, Khan WA, Irfan M, Sultan F, Shahzed M, Khan M (2019a) Computational analysis of entropy generation for cross-nanofluid flow. Appl Nanosci. https://doi.org/10.1007/s13204-019-01038-w

Ali M, Sultan F, Khan WA, Shahzad M (2019b) Exploring the physical aspects of nanofluid with entropy generation. Appl Nanosci. https://doi.org/10.1007/s13204-019-01173-4
Ali M, Sultan F, Khan WA, Shahzad M, Arif H (2020) Important features of expanding/contracting cylinder for cross magneto-nanofluid flow. Chaos, Solitons Fractals 133:109656
Anwar MS, Rasheed A (2018) Joule heating in magnetic resistive flow with fractional Cattaneo–Maxwell model. J Braz Soc Mech Sci Eng. https://doi.org/10.1007/s40430-018-1426-8
Asghar Z, Ali N, Ahmed R, Waqas M, Khan WA (2019) A mathematical framework for peristaltic flow analysis of non-Newtonian Sisko fluid in an undulating porous curved channel with heat and mass transfer effects. Comput Methods Program Biomed 182:105040
Chaudhary MA, Merkin JH (1995) A simple isothermal model for homogeneous–heterogeneous reactions in boundary-layer flow. I. Equal diffusivities. Fluid Dyn Res 16:311–333
Deng W, Yao R, Zhao H, Yang X, Li G (2017a) A novel intelligent diagnosis method using optimal LS-SVM with improved PSO algorithm. Soft Comput. https://doi.org/10.1007/s00500-017-2940-9
Deng W, Zhao H, Zou L, Li G, Yang X, Wu D (2017b) A novel collaborative optimization algorithm in solving complex optimization problems. Soft Comput 21(15):4387–4398
Deng W, Zhao H, Yang X, Xiong J, Sun M, Li B (2017c) Study on an improved adaptive PSO algorithm for solving multi-objective gate assignment. Appl Soft Comput 59:288–302
Deng W, Xu J, Zhao H (2019) An improved ant colony optimization algorithm based on hybrid strategies for scheduling problem. IEEE Access 7:20281–20292
Haq I, Shahzad M, Khan WA, Irfan M, Mustafa S, Ali M, Sultan F (2019) Characteristics of chemical processes and heat source/sink with wedge geometry. Case Stud Therm Eng 14:100432
Hayat T, Rashid M, Alsaedi A (2018) Three dimensional radiative flow of magnetite-nanofluid with homogeneous–heterogeneous reactions. Results Phys 8:268–275
Hei Y, Zhang C, Song W, Kou Y (2019) Energy and spectral efficiency tradeoff in massive MIMO systems with multi-objective adaptive genetic algorithm. Soft Comput 23:7163–7179
Imtiaz M, Mabood F, Hayat T, Alsaedi A (2019) Homogeneous–heterogeneous reactions in MHD radiative flow of second grade fluid due to a curved stretching surface. Int J Heat Mass Transf 145:118781
Irfan M, Khan M, Khan WA (2018) Interaction between chemical species and generalized Fourier's law on 3D flow of Carreau fluid with variable thermal conductivity and heat sink/source: a numerical approach. Results Phys 10:107–117
Khan WA, Khan M, Alshomrani AS, Ahmad L (2016) Numerical investigation of generalized Fourierís and Fickís laws for Sisko fluid flow. J Mol Liq 224:1016–1021
Khan M, Irfan M, Khan WA, Alshomrani AS (2017) A new modeling for 3D Carreau fluid flow considering nonlinear thermal radiation. Results Phys 7:2692–2704
Khan M, Irfan M, Khan WA, Ayaz M (2018) Aspects of improved heat conduction relation and chemical processes on 3D Carreau fluid flow. Pramana J Phys. https://doi.org/10.1007/s12043-018-1579-0
Khan WA, Ali M, Sultan F, Shahzad M, Khan M, Irfan M (2019a) Numerical interpretation of autocatalysis chemical reaction for nonlinear radiative 3D flow of cross magnetofluid. Pramana J Phys. https://doi.org/10.1007/s12043-018-1678-y
Khan WA, Sultan F, Ali M, Shahzad M, Khan M, Irfan M (2019b) Consequences of activation energy and binary chemical reaction for 3D fow of Cross-nanofluid with radiative heat transfer. J Braz Soc Mech Sci 41:4. https://doi.org/10.1007/s40430-018-1482-0
Khan WA, Ali M, Sultan F, Shahzad M, Khan M, Irfan M (2019c) Numerical interpretation of autocatalysis chemical reaction for nonlinear radiative 3D flow of cross magnetofluid. Pramana J Phys 92:16. https://doi.org/10.1007/s12043-018-1678-y
Mahanthesh B, Gireesha BJ, Shashikumar NS, Hayat T, Alsaedi A (2018) Marangoni convection in Casson liquid flow due to an infinite disk with exponential space dependent heat source and cross-diffusion effects. Results Phys 9:78–85
Mahdy A (2019) Aspects of homogeneous-heterogeneous reactions on natural convection flow of micropolar fluid past a permeable cone. Appl Math Comput 352:59–67
Malik R, Khan M (2018) Numerical study of homogeneous-heterogeneous reactions in Sisko fluid flow past a stretching cylinder. Results Phys 8:64–70
Merkin JH (1996) A model for isothermal homogenous-heterogeneous reactions in boundarylayer flow. Math Comput Model 24:125–136
Muhammad S, Ali G, Shah SIA, Irfan M, Khan WA, Ali M, Sultan F (2019) Numerical treatment of activation energy for the three-dimensional flow of a cross magnetonanoliquid with variable conductivity. Pramana J Phys 93:40. https://doi.org/10.1007/s12043-019-1800-9
Rashid M, Hayat T, Rafique K, Alsaedi A (2019) Chemically reactive flow of thixotropic nanofluid with thermal radiation. Pramana J Phys. https://doi.org/10.1007/s12043-019-1837-9
Shahzad M, Ali M, Sultan F, Khan WA, Hussain Z (2020) Computational investigation of magneto-cross fluid flow with multiple slip along wedge and chemically reactive species. Results Phys 16:102972
Shen M, Chen L, Zhang M, Liu F (2018) A renovated Buongiorno's model for unsteady Sisko nanofluid with fractional Cattaneo heat flux. Int J Heat Mass Transf 126:277–286
Soomro FA, Usman M, Haq RU, Wang W (2018) Melting heat transfer analysis of Sisko fluid over a moving surface with nonlinear thermal radiation via collocation method. Int J Heat Mass Transf 126:1034–1042
Sultan F, Khan WA, Ali M, Shahzad M, Irfan M, Khan M (2019a) Theoretical aspects of thermophoresis and Brownian motion for three-dimensional flow of the cross fluid with activation energy. Pramana J Phys 92:21. https://doi.org/10.1007/s12043-018-1676-0
Sultan F, Khan WA, Ali M, Shahzad M, Sun H, Irfan M (2019b) Importance of entropy generation and infinite shear rate viscosity for non-Newtonian nanofluid. Int J Mech Sci 41:439. https://doi.org/10.1007/s40430-019-1950-1
Toghraie D, Esfahani NN, Zarringhalam M, Shirani N, Rostami S (2020) Blood flow analysis inside different arteries using non-Newtonian Sisko model for application in biomedical engineering. Comput Methods Program Biomed. https://doi.org/10.1016/j.cmpb.2020.105338
Waqas M (2020) A mathematical and computational framework for heat transfer analysis of ferromagnetic non-Newtonian liquid subjected to heterogeneous and homogeneous reactions. J Mag Mag Mater 493:165646
Waqas M, Jabeen S, Hayat T, Khan MI, Alsaedi A (2019) Modeling and analysis for magnetic dipole impact in nonlinear thermally radiating Carreau nanofluid flow subject to heat generation. J Magn Magn Mater. https://doi.org/10.1016/j.jmmm.2019.03.040
Xu NL, Xu H, Raees A (2018) Homogeneous–heterogeneous reactions in flow of nanofluids near the stagnation region of a plane surface: the Buongiorno's model. Int J Heat Mass Transf 125:604–609
Zhang S, Zhao H, Xu J, Deng W (2019) A novel fault diagnosis method based on improved adaptive VMD energy entropy and

PNN. Trans Can Soc Mech Eng. https://doi.org/10.1139/tcsme-2018-0195

Zhao H, Deng W, Li G, Lifeng Y, Bing Y (2016) Research on a new fault diagnosis method based on WT, improved PSO and SVM for motor. Recent Patents Mech Eng 9:289–298

Zhao H, Sun D, Deng W, Yang X (2017) A new feature extraction method based on EEMD and multi-scale fuzzy entropy for motor bearing. Entropy. https://doi.org/10.3390/e19010014

Zhao H, Zheng J, Xu J, Deng W (2019a) Fault diagnosis method based on principal component analysis and broad learning system. IEEE Access 7:99263–99272

Zhao H, Liu H, Xu J, Deng W (2019b) performance prediction using high-order differential mathematical morphology gradient spectrum entropy and extreme learning machine. IEEE Trans Instrum Meas. https://doi.org/10.1109/TIM.2019.2948414

Zhao H, Zheng J, Deng W, Song Y (2020) Semi-supervised broad learning system based on manifold regularization and broad network. IEEE Trans Circuits Syst I Regul Pap 67(3):983–994